International Journal of Concrete Structures and Materials

RESEARCH Open Access

Effects of Gamma-Ray Irradiation on Hardened Cement Mortar

Yuliia Khmurovska[1], Petr Štemberk[2*], Svyatoslav Sikorin[2], Jiří Němeček[3], Daria Jóźwiak-Niedźwiedzka[4], Magdaléna Doleželová[5], Yuliya Kaladkevich[6], Eryk Pavalanski[6] and Viktar Fatseyeu[6]

Abstract

The effect of gamma-ray irradiation on cement mortar properties is investigated in this study in order to understand the mechanism behind the strength and stiffness reduction, which may be significant according to the available researches. ^{60}Co irradiation facility with the generating dose rate of 0.1–10 Gy/s and the total activity of $4.4 \cdot 10^{15}$ Bq (120 kCi) was used to perform the irradiation, so that the total observed dose of the irradiated samples reached the values ranging from 12.0 to 15.0 MGy. An identical set of control samples was placed in the same laboratory conditions away from gamma radiation. The results of nanoindentation, X-ray diffraction analysis and mercury intrusion porosimetry of the irradiated and the control samples are shown and explained in detail in this study. The nanoindentation creep compliance and the nanoindentation elastic modulus of the irradiated and the control samples do not show any significant difference. The mineral composition obtained using the X-ray diffraction analysis of the irradiated and the control samples is also similar. The pore structure rearrangement and microcrack occurrence, which were evidenced by the mercury intrusion porosimetry and scanning electron microscopy, led to the porosity increase and may be attributed to the significant decrease of compressive strength.

Keywords: cement mortar, drying, experiment, gamma-ray, nanoindentation, porosity, X-ray diffraction

1 Introduction

Concrete structures and elements, such as biological shields of nuclear power plants, irradiation facility walls and casks for radioactive waste storage, may be exposed to long-term ionizing radiation (Vaitová et al. 2018; Khmurovska et al. 2019a). The two major types of radiation which affect concrete are neutron radiation and gamma-ray radiation, whereas the neutron irradiation is always accompanied by the effect of gamma-rays. For the concrete structures, such as gamma-irradiation facility walls or casks for radioactive waste storage, the effect of neutron irradiation is absent or is negligibly small, therefore, the influence of gamma-ray irradiation on these structures becomes critical.

Regarding the long-term performance, the knowledge of possible changes in strength and creep, which are mainly affected by gamma-ray radiation, becomes essential. Since the experimental data on the effect of gamma-ray radiation on concrete are rather scarce, or even contradictory, this paper tries to help fill in the gaps by joining the global effort in this field (McDowall 1971; Gray 1972; Denisov et al. 2012; Dubrovskii 2010; Hilsdorf et al. 1978; Lowinska-Kluge and Piszora 2008; Soo and Milian 2001; Vodák et al. 2005; Vodák et al. 2011; Maruyama et al. 2017; Maruyama et al. 2018; Khmurovska et al. 2019b; Reches 2019a; Tajuelo et al. 2018, etc.).

The homogeneity of information can be assessed from the following short literature review. For example, according to the research published by Khmurovska et al. (2019b), the creep of irradiated cement mortar samples is slightly higher, nonetheless the creep and the

*Correspondence: stemberk@fsv.cvut.cz
[2] Laboratory of Experimental Physics and Nuclear Safety of Reactor Facilities, The Joint Institute for Power and Nuclear Research, Sosny of the National Academy of Sciences of Belarus, 220109 Minsk, Belarus
Full list of author information is available at the end of the article
Journal information: ISSN 1976-0485 / eISSN 2234-1315.

shrinkage lie within the interval predicted by the common structural prediction models (Bažant and Jirásek 2018; CEB-FIP 1991; Taerwe and Matthys 2013; ACI Code Committee 2008; Gardner and Lockman 2001) for both the irradiated and the control samples. However, according to another available research of the effect of gamma-ray irradiation on the creep of cement paste on macro-level (McDowall 1971), the gamma-rays reduce creep but increase autogenous shrinkage, nevertheless, McDowall (1971) believes that the difference may become insignificant in the course of time. The effect of gamma-ray irradiation on cement paste creep on micro- and nano-level was investigated by Tajuelo et al. (2018), Tajuelo et al. (2020), Hilloulin et al. (2018) and Robira et al. (2018). All these studies reported that the creep of irradiated samples is slightly lower or equal to that of control samples, however, it should be noted that in all cases the total absorbed dose was quite low (< 1 MGy).

Also, according to Khmurovska et al. (2019b), the cement mortar strength is reduced by 20% on average under the exposure to gamma-ray irradiation with the total absorbed dose of 12.0–15.0 MGy; see Fig. 1. The strength reduction seems to be high in comparison to the other researches. For example, according to Hilsdorf et al. (1978), a significant reduction of the cement paste properties is expected to appear only beyond the threshold of the absorbed gamma-ray dose of 200 MGy. Also, Lowinska-Kluge and Piszora (2008) identified the decomposition of hydrates within the absorbed gamma-ray dose range of 130–836 MGy, which may lead to degradation of concrete properties. On the other hand, Maruyama et al. (2017) observed an increase in concrete strength with the absorbed dose of up to 200 MGy due to carbonation reaction and concluded that the effect of gamma-ray irradiation is equivalent to that of heating and drying. This is contradicted by Soo and Milian (2001) and Vodák et al. (2005) who observed a reduction in compressive strength at much lower absorbed gamma-ray dose (15% reduction at the absorbed dose of 22 MGy and 10% reduction at the absorbed dose of 0.3–0.5 MGy). However, Reches (2019a) noticed that the results of Soo and Milian (2001) have anomalous variation with respect to time after casting. The magnitude of the variation is comparable to the reported effect of irradiation. Also, the statistics of such experiments as Soo and Milian (2001) and Vodák et al. (2005) are usually poor (one or two samples) because of the limited number of samples which can be irradiated in relatively small irradiation chambers. Robira et al. (2018) found that the effect of gamma-ray irradiation on cement paste strength is rather insignificant, however, the effect of gamma-ray irradiation on strength of cement mortar is essential (4% decrease of compressive strength and 15% decrease of flexural strength) even despite the low total absorbed dose (0.257 MGy). Moreover, Robira et al. (2018) reported no significant decrease in strength for carbonated cement mortar samples. This shows an important role of carbonation and indicates that the environmental conditions of the experiment should be properly described since the strength of cement mortar can be varied not only by irradiation, but also by favorable/unfavorable carbonation conditions. Nevertheless, the majority of the available researches claim low or insignificant effect of gamma-ray irradiation on concrete strength beyond statistical noise.

It should be emphasized that all the above described researches used different materials, mixture proportions and sample sizes. Dose rates, total absorbed doses, environmental temperature and relative humidity also differed. As all these factors may affect concrete properties, the available experimental results cannot be simply compared.

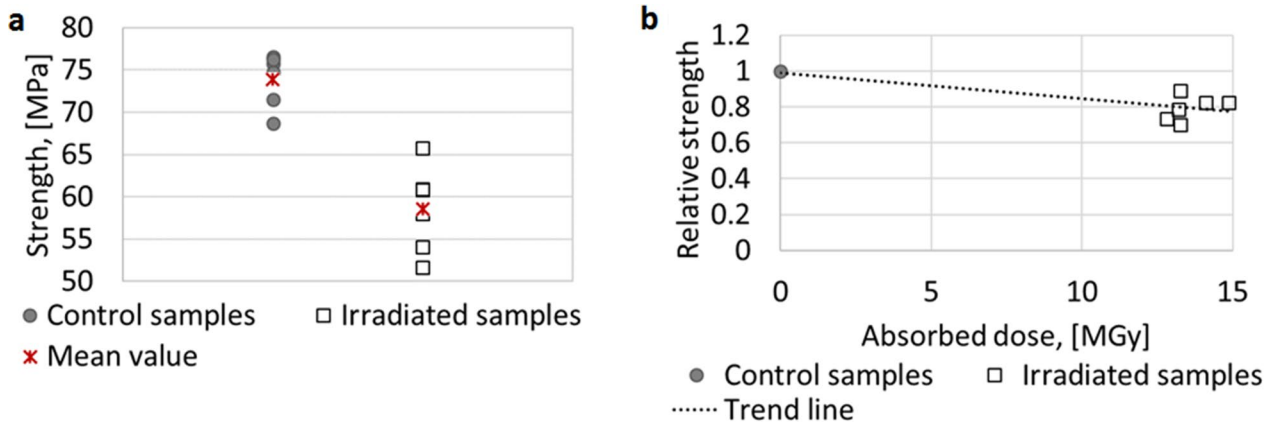

Fig. 1 Compressive strength of cement mortar samples (Khmurovska, 2019b): **a** in MPa, **b** relative in dependence on absorbed irradiation dose.

This paper presents supplementary measurements intended to clarify the available results and to extend the results published primarily by Khmurovska et al. (2019b); see Fig. 1, when all the measurements were carried out using the samples of the same geometry and composition. The supplementary measurements help to explain the observed radiation-induced changes and thus, they create a full set of experimental data, which are needed in the numerical simulations of gamma-ray irradiation critical concrete structures. The supplementary measurements presented in this paper are the creep measurement using nanoindentation, elastic indentation modulus measurement, X-ray diffraction (XRD) analysis and mercury intrusion porosimetry (MIP). The measurements help to quantify how creep and strength of cement mortar are affected by gamma-ray irradiation.

2 Experiment and Post-irradiation Examination

The mortar composition was selected so that it corresponds to the standard structural concrete composition used in the Czech NPPs without the addition of coarse aggregates. Therefore, the mortar consists of CEM I 42.5R cement with water–cement ratio of 0.38, 0—4 mm siliceous aggregates and a polycarboxylate-based superplasticizer. The test samples were small-scale with the dimensions of $10 \times 10 \times 40$ mm. The detailed mixture composition is given in Table 1, where weight is shown in as-used conditions, and is identical to that used in (Khmurovska et al. 2019b). The weight of the fine siliceous aggregates in the saturated surface dry (SSD) state is shown in Table 1 in the brackets.

All the test samples were prepared under controlled temperature of 20 °C and were cured in water for 10 days. Then, the samples were stored under the same controlled temperature in a sealed condition for 62 days until the beginning of the experiment. The sealed condition (insulation) was provided by three layers of polyethylene foil in order to ensure sufficient curing and to eliminate drying shrinkage. After curing, the insulation was removed and the dimension and weight measurements of all the samples were conducted. The average sample volume was 3981 mm^3 (the standard deviation was 182.8 mm^3), while the average sample weight was 9.26 g (the standard deviation was 0.41 g). Thus, the average density of the samples at the beginning of experiment was equal to 2326 kg/m^3 (the standard deviation was 36.3 kg/m^3).

Table 1 Composition of mortar.

Component	Weight
Cement (CEM I 42.5R)	1000 g
Water	380 g
Siliceous aggregates with fraction of 0–4 mm (SSD)	1600 g (1613 g)
Superplasticizer (Glenium ACE 442)	9.5 g

The samples were loaded and irradiated just after the dimension and weight measurements, which followed the isolation removal. The load was applied by compressing the loading spring. The stiffness of the loading spring was chosen in the way that 1 cm of spring compression created a force equal to 0.5 kN. Two load levels of 1.0 kN and 1.5 kN (10 and 15 MPa, respectively) were considered, which are approximately equal to the stress level of 13.5 and 20% of compressive strength, respectively. The load levels were chosen so that representative results regarding the possible effect of constraint condition in the concrete mass could be obtained while the samples would not be damaged by the load during the test. Not loaded samples were also investigated. 14 samples in total were irradiated (5 not loaded, 4 under 1.0 kN load and 5 under 1.5 kN load) and an identical set of control samples was placed in the same laboratory conditions away from gamma-ray radiation.

^{60}Co Irradiation Facility UGU-420 of The Joint Institute for Power and Nuclear Research—Sosny of the National Academy of Sciences of Belarus in Minsk with the generating dose rate of 0.1–10 Gy/s and the total activity of $4.4 \cdot 10^{15}$ Bq (120 kCi) was used to carry out the experiments. The radiation dose rate was in the range from 3.90 to 4.71 kGy/h. The average irradiation time was 8.6 h per day. The total absorbed dose after 369 days of irradiation varied from 12.0 to 15.0 MGy for different samples depending on the activity and distance to each irradiation source (768 sources in total) facing the individual sample. The position of the samples in the irradiation chamber was fixed during the whole experiment. The experiment is explained schematically in Fig. 2.

The temperature and the relative humidity in the irradiation chamber (when not in operation) and in the laboratory were recorded. It should be noted that the temperature and the relative humidity in the irradiation chamber and laboratory were exactly the same. The measured relative humidity and the temperature together with the trendlines and indication of the seasons are shown in Fig. 3. A lower relative humidity in winter and spring corresponds to the heating period in the facility. The overall average temperature during the irradiation was 16.2 ℃ (the standard deviation was 4.16 ℃) and the average relative humidity was 50% (the standard deviation was 12.29%).The weight of the not loaded samples was measured using a high-precision laboratory scale with an error of ± 0.002 g. The measurements were carried out once a day during the first week of the experimental investigation, three times per

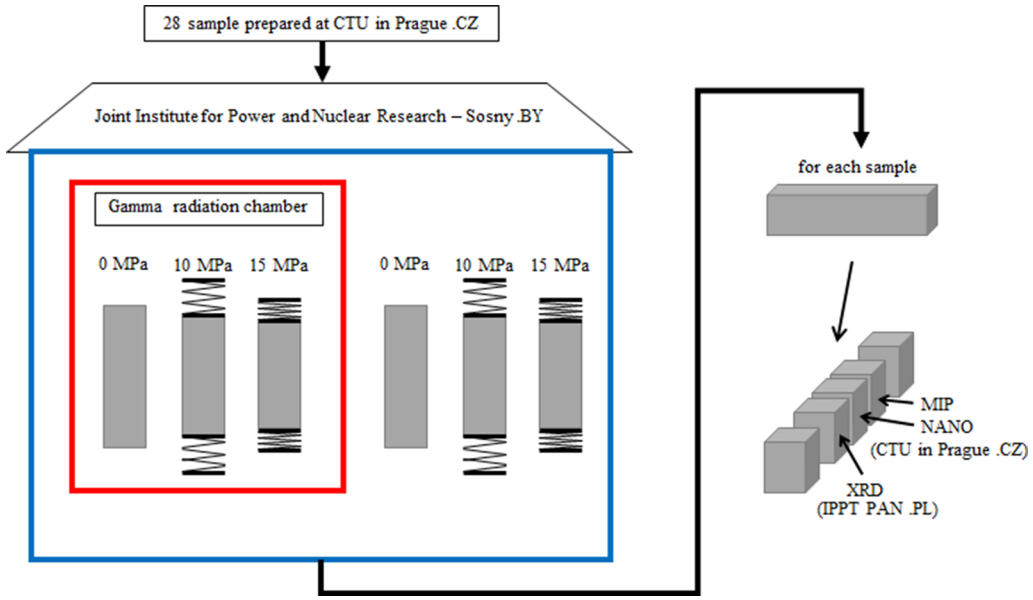

Fig. 2 Schematic description of experiment, where "Nano" stands for nanoindentation.

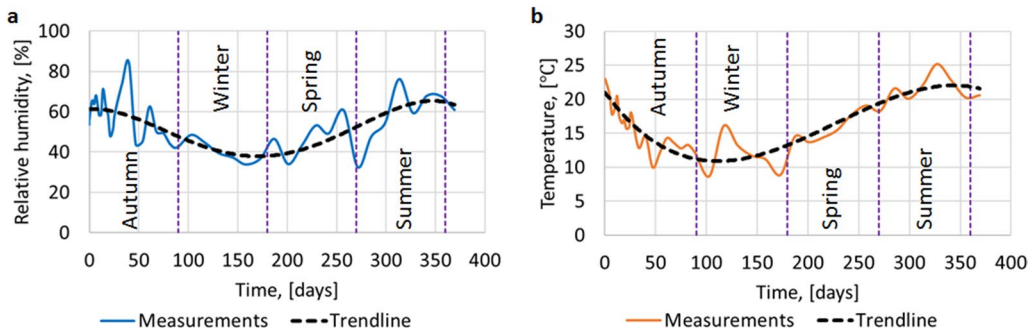

Fig. 3 Environmental conditions: **a** relative humidity, **b** temperature.

week during the next 3 weeks, once per week during the next 2 months and once per 2 weeks during the rest of the experimental investigation.

After the irradiation, at least one sample from each set (not loaded, 1.0 kN and 1.5 kN loaded irradiated samples, and not loaded, 1.0 kN and 1.5 kN loaded control samples) were cut into 5 sections by a precision cut-off machine Brillant 210 with a diamond blade; see Figs. 2 and 4. The sample sections from the sample ends were not used in further analyses in order to exclude any chance of the edge effect with respect to production and drying process. The intermediate sections were used for the nanoindentation, powder X-ray diffraction (XRD) analysis and the mercury intrusion porosimetry (MIP) test.

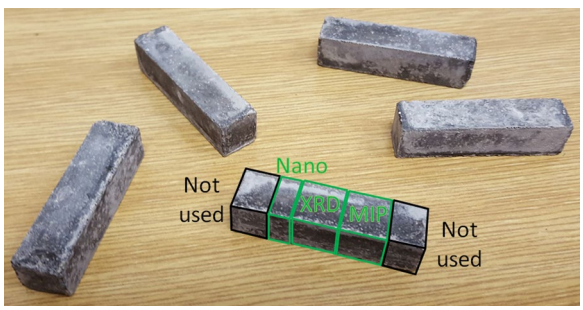

Fig. 4 Samples with schematic depiction of sections, where "Nano" stands for nanoindentation.

The surface of the sample sections, which were used for nanoindentation, was polished with silicon carbide paper with the grit size of P2000 and P4000, according to FEPA Standards. The polished sample section is shown in Fig. 5a. The nanoindentation of the polished sample sections was carried out with a Hysitron Tribolab Ti-700 with the Berkovich diamond tip. Six grids of 8×8 indents with the spacing of 6 μm were predetermined on the surface of each sample in order to avoid aggregates; see Fig. 5b. The aggregates were avoided by visual observation using the optical microscope, which the nanoindenter is equipped with. The microscope magnification allows to distinguish between the cement paste and the aggregates. Also, the surface roughness was measured using Hysitron Tribolab Ti-700 piezo scanner before each individual grid measurement and was characterized by the root-mean-square parameter. The achieved roughness was 20—50 nm. The air indent calibration was conducted before each measurement. The nanoindentation was performed in the laboratory with the controlled environmental temperature of 22 °C and relative humidity of 50%.

The nanoindentation loading process is shown schematically in Fig. 6a. The nanoindentation was performed using the load-controlled test with the trapezoidal loading diagram; see Fig. 6b. The sample surface was loaded linearly by the Berkovich diamond tip during 1 s till the maximum force of 3000 μN was reached, which was followed by 40 s of holding period and 1 s of unloading in order to evaluate the indentation creep compliance. The loading and unloading rates were 3000 μN/s.

Additionally to the nanoindentation, the scanning electronic microscopy (SEM) of the same sample sections was performed. SEM-BSE images were captured by Phenom XL desktop scanning electron microscope at an accelerating voltage of 15 kV and magnification of 2000×; see Fig. 5b.

The sample sections which were used for the XRD analysis were powdered and sieved through a 0.045-mm sieve. The fraction of the material which did not pass through the sieve was powdered and sieved again. The procedure was repeated until more than 90% of the sample material was properly powdered and sieved. The randomly oriented powder mount technique was then applied. The Bruker D8 DISCOVER diffractometer (at Institute of Fundamental Technological Research of Polish Academy of Science, IPPT PAN) with a voltage ratio of 40 kV and 40 mA lamp current was used. The copper lamp served as an X-ray source (radiation CuKα with a wavelength 0.1542 nm). The measurements were carried out in the reflection mode, using the Bragg–Brentano geometry with a 1-mm gap and two 2.5° sollers on the primary and the secondary side. The angular ranging of 2θ measurements ranged from 5° to 65°, with a 0.02° step and a counting time of 1 s per step.

The sample sections which were used for the porosity evaluation were dried in an oven at 50 °C for 3 days and then they were broken into pieces. A total of 12 samples were investigated (3 not loaded, 3 loaded irradiated samples, and 3 not loaded, 3 loaded control samples) by MIP. The center pieces without significantly large aggregates were selected for further porosity investigation by the mercury porosimeter PASCAL 140/440 with the pressure range from 0.005 to 400 MPa.

3 Results and Discussion

3.1 Change in Relative Weight

The change in relative weight of the not loaded irradiated samples and the control samples together with the trendlines is shown in Fig. 7. The loaded samples could not be measured as they were compressed continuously. The plot of the ambient relative humidity trendline is also shown in Fig. 7. As can be seen, the relative weight is strongly affected by the ambient relative humidity in the

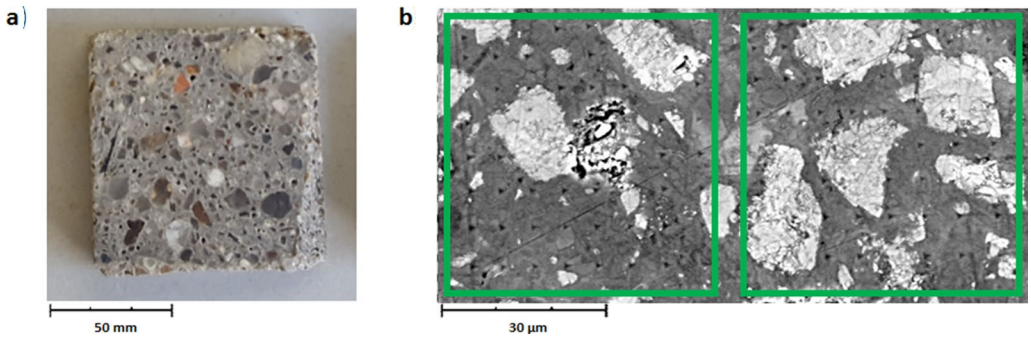

Fig. 5 Sample section used for nanoindentation: **a** sample surface, **b** SEM image with visible indents, where green squares indicate two individual grids.

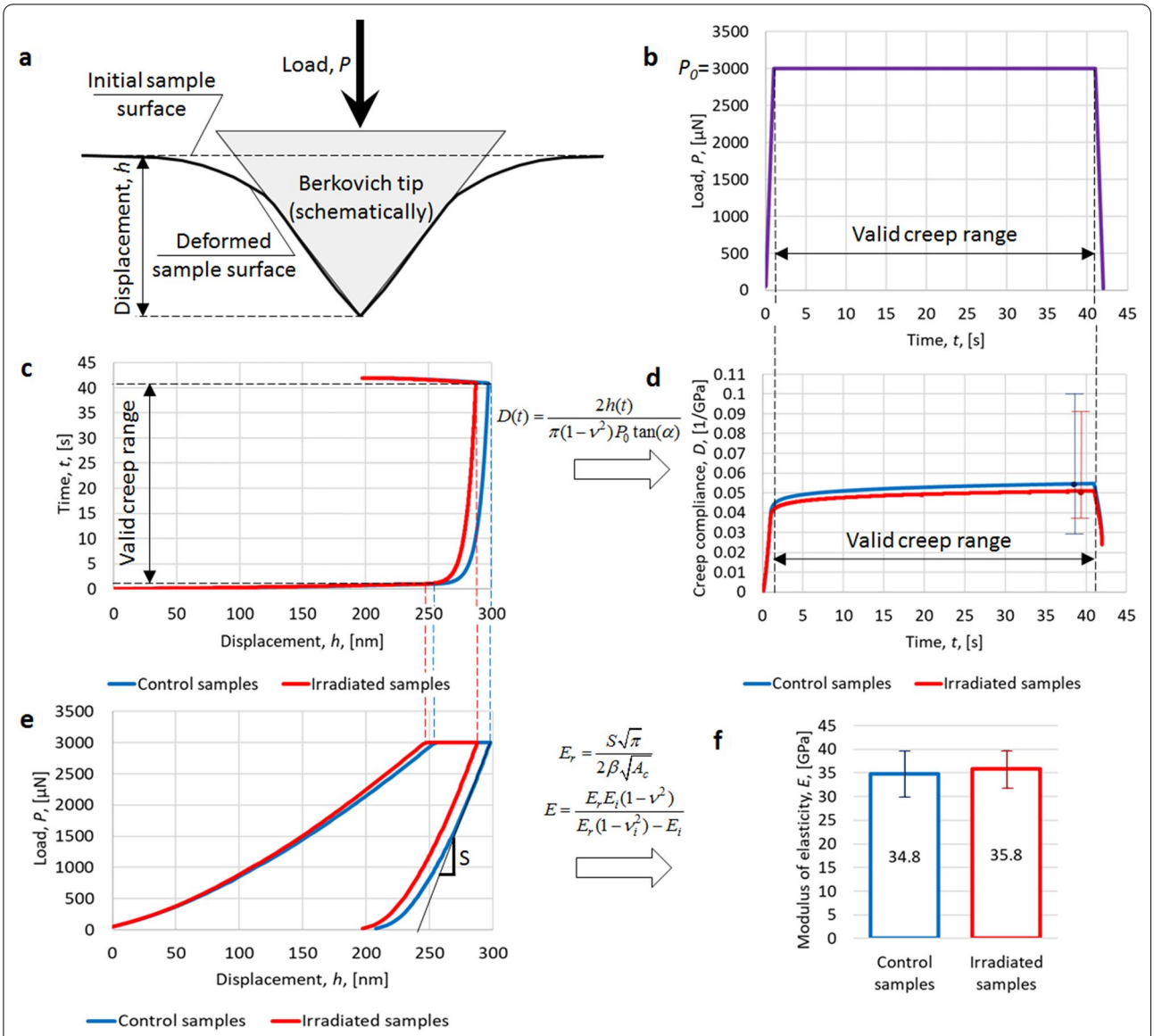

Fig. 6 Nanoindentation: **a** schematic description, **b** loading diagram, **c** average time–displacement curves of C–S–H gel, **d** average creep compliance of C–S–H gel, **e** average load–displacement curves of C–S–H gel, **f** average indentation elastic modulus of C–S–H gel.

facility, when with higher humidity the relative weight becomes higher, and vice versa. However, the irradiated samples have smaller relative weight in comparison to the control samples which may indicate additional drying due to dehydration caused by water radiolysis and/or water evaporation caused by gamma heating.

3.2 Indentation Creep Compliance

The results of the nanoindentation focus on the C–S–H gel phase since this phase is responsible primarily for the creep of cement paste.

The C–S–H gel phase was identified based on the following procedure: firstly, the indentation elastic modulus of all the indents was calculated (see Sect. 3.3 for details on the indention elastic modulus calculation). Then, it was considered that the indents with the elastic modulus lower than 40 GPa may belong to the C–S–H gel phase; see Fig. 8a, where the indentation elastic moduli of all the indents are shown. After that, all the indents were additionally checked by SEM, since it is known that the C–S–H gel phase has dark gray color in SEM-BSE images. The final confirmation regarding the phase identification was made based on the SEM

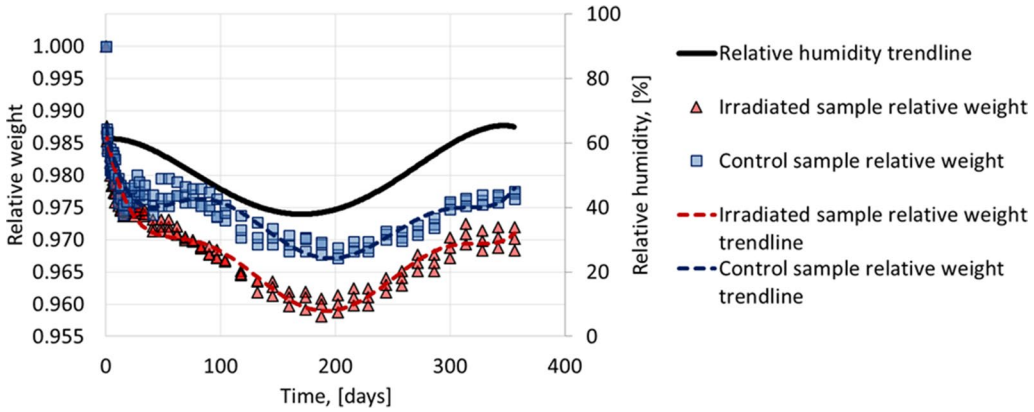

Fig. 7 Change in relative weight.

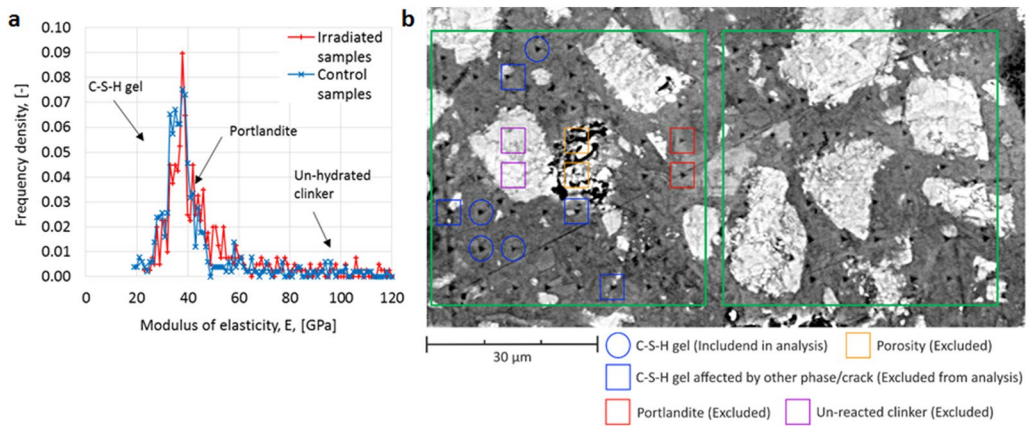

Fig. 8 Phase identification procedure: **a** indentation elastic moduli, **b** SEM phase identification, where green squares indicate two individual grids.

observation as shown in Fig. 8b. Also, the indentation curves with the drift rate higher than 0.05 nm/s were excluded from the results in order to minimize the error in the creep measurement during the holding period.

The indentation creep compliance was calculated for the C–S–H gel phase only. The calculation was done using the time–displacement curves, which were obtained during the nanoindentation. The average time–displacement curves for control samples (270 valid C–S–H gel tests in total) and irradiated samples (175 valid C–S–H gel tests in total) are shown in Fig. 6c. Assuming a constant load, the indentation creep compliance was calculated according to the following formula (Shimizu et al. 1999):

$$D(t) = \frac{2h^2(t)}{\pi(1-\nu^2)P_0 \tan(\alpha)}, \quad (1)$$

where $D(t)$ is the creep compliance in 1/GPa over time t in s, $h(t)$ is the indentation depth in nm over time t in s (displacement over time), P_0 is the constant load equal to 3000 µN, υ is the Poisson's ratio of the tested material, which was considered equal to 0.2, and α is an angle between the surface and the edge of the tip (α is equal to 19.7° for the equivalent to the Berkovich diamond tip conical indenter) (Oliver and Pharr 2004; Minster et al. 2010; Shimizu et al. 1999).

Since the sample cannot be loaded instantly, the values of the indentation creep compliance during the first and the last seconds should not be taken into consideration. The valid creep range is shown in Fig. 6b–d.

The obtained average creep compliance of the control and the irradiated samples as well as the data scatter are shown in Fig. 6d. The results show that the irradiation-induced change in the indentation creep compliance remains within the respective data scatter. Since, the

data scatter of the control and the irradiation samples are also very similar, it can be concluded that the effect of gamma-ray irradiation on cement paste creep is insignificant even at nano-level.

3.3 Indentation Elastic Modulus

The indentation elastic moduli of all the indents were calculated from the load–displacement curves and are shown in Fig. 8a. The indentation elastic modulus was determined using the Oliver and Pharr theory (Oliver and Pharr 1992) according to the following formulas:

$$E_r = \frac{S\sqrt{\pi}}{2\beta\sqrt{A_c}}, \tag{2}$$

$$E = \frac{E_r E_i(1-\nu^2)}{E_r(1-\nu_i^2) - E_i}, \tag{3}$$

where S is the rigidity of the contact defined as the slope of the initial section of the unloading curve $S = dP/dh$, see Fig. 6e, β is the tip geometry coefficient, which is equal to 1.034 for Berkovich tip, A_c is the indent projection area, υ_i is the Poisson's ratio of the diamond indenter tip, which is equal to 0.07, υ is the Poisson's ratio of the tested material, which was considered to be equal to 0.2, E_r is the reduced elastic modulus, E_i is the elastic modulus of the diamond indenter tip, which is equal to 1140 GPa, and E is the elastic modulus of the tested material.

The results presented below focus on the C–S–H gel phase only. The average load–displacement curves of the C–S–H gel indents for control (270 valid C–S–H gel tests in total) and irradiated samples (175 valid C–S–H gel tests in total) are shown in Fig. 6e.

The obtained average elastic modulus of the C–S–H gel and the corresponding standard deviation (the confidence level of 95%) of the control and the irradiated samples are shown in Fig. 6f. The difference between the obtained elastic moduli is minor and remains within the standard deviation range which indicates that gamma-ray irradiation does not cause any significant change in C–S–H gel on the nano-level.

3.4 XRD

The diffraction patterns represent the results of the XRD analysis. The qualitative analysis based on the obtained X-ray profiles was made using EVA v.3 evaluation program with a database provided by the manufacturer. The background and the amorphous halo have been subtracted in the evaluation program and are described below, while the raw data are shown in the Additional files 1, 2, 3, 4, 5, 6, 7, 8 section. The diffraction patterns of the samples (irradiated and control) and the aggregates with the denoted principal characteristic peaks (alite, belite, portlandite, ettringite, quartz, albite and orthoclase) are shown in Fig. 9.

The qualitative analysis of the obtained diffraction patterns shows an insignificant variation in the control and

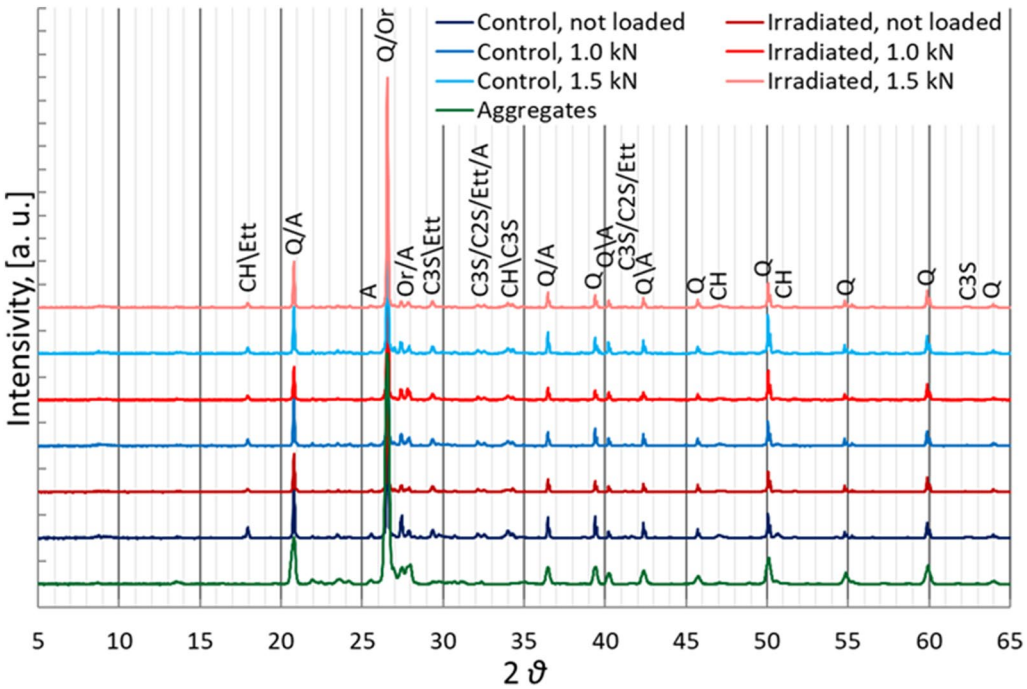

Fig. 9 Sample and aggregate diffraction patterns (C3S: alite; C2S: belite CH: portlandite; Ett: ettringite; Q: quartz; A: albite; Or: orthoclase).

the irradiated sample mineral composition. In the presented research, the mortars have been analyzed using XRD and the strong peaks from sand minerals could affect slightly the peaks coming from the cement matrix. Therefore, the fine aggregate itself was analyzed in order to isolate the peaks derived from the minerals in the quartz sand.

Based on the XRD analysis, it can be concluded that there is no significant effect of gamma-ray irradiation on the analyzed sample mineral composition. The carbonation products (calcite, aragonite, vaterite) were not detected using the prescribed experimental method, although other researchers (Vodák et al. 2011; Maruyama et al. 2017, 2018) observed the effect of gamma-ray irradiation on the occurrence of cement paste carbonation, their test conditions were different: various radiation doses, material composition, curing and environmental conditions. In this study, the low water–cement ratio (0.38) in comparison to the other researches (Vodák et al. 2011; Maruyama et al. 2017, 2018) can reduce the rate of carbonation reaction. Also, the fact that the temperature during approximately 9 months out of 12 months of irradiation was quite low (lower than 20 °C, see Fig. 3b, may also slow down the carbonation reaction, since the carbonation depth increases with the temperature increase (Chen et al. 2018). In addition, based on the available research (Elsalamawy et al. 2019), the highest carbonation depth may be observed in the relative humidity 60–70%. In the present study, the relative humidity was lower than 60–70% during almost 10 months out of 12 months of irradiation, see Fig. 3a, and this may have also reduced the rate of carbonation reaction. However, it should be noted that it was possible that some amount of carbonation products, which was beyond the sensitivity limit of the experimental method, was present but was not detected. Nevertheless, the irradiation-induced acceleration of natural carbonation or carbonation of the sample core, which was reported by Vodák et al. 2011, was not detected in this study using the above explained experimental method for the environmental conditions, which are shown in Fig. 3.

3.5 MIP

The pore size distribution, which was obtained using the MIP technique, differs not only for the control and the irradiated samples, but also for the samples subjected to long-term loading (1.0 and 1.5 kN) and the not loaded samples. Thus, the MIP results for these samples are shown separately in this section.

The total porosity of the loaded, the not loaded, the control and the irradiated samples is shown in Fig. 10. Generally, the sustained load can simultaneously both increase porosity due to the uneven creep of mortar components and decrease porosity by closing the microcracks. In this study, the higher porosity of the control loaded samples, in comparison to the control not loaded samples, can be explained by unequal creep of cement paste and aggregates which results in tensile stresses and leads to the fracture of gel pores. On the other hand, the irradiated samples have similarly high total porosity (> 10%) regardless of the load. This means that the cement paste structure was fractured by the effect of irradiation, not by the load, and the effect of uneven creep and pore closing effect are similar in magnitude. This is believed to make the effect of the load of irradiated samples insignificant in terms of the total porosity.

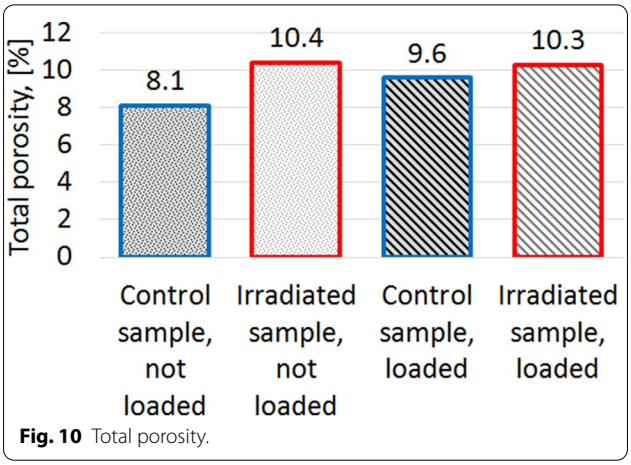

Fig. 10 Total porosity.

Nevertheless, the total porosity of the control samples is in accordance with the previously published results (Nokken and Hooton 2008) for both the not loaded and the loaded samples. However, the total porosity of the irradiated samples is higher and rather corresponds to the previously published results for dried samples (Nokken and Hooton 2008). This can be explained by the water evaporation caused by gamma heating. Additional dehydration can be caused by radiolytic decomposition of water with subsequent evaporation of the radiolysis products. Therefore, the irradiation, similarly to drying, leads to the increase in porosity due to the microcrack occurrence. The microcracks of the irradiated samples were observed by the SEM investigation and are evidenced in Fig. 11a and b, however, no significant microcracks were observed in the control samples; see Fig. 11 c and d. In Fig. 11a, the microcracks which are radial to the aggregates can be seen, while Fig. 11b shows the microcrack along aggregate perimeter. Such types of cracks may appear due to the uneven dehydration of cement paste and aggregates. For bigger samples with a higher effect of gamma heating, the uneven thermal expansion of cement mortar constituents may also cause additional cracking

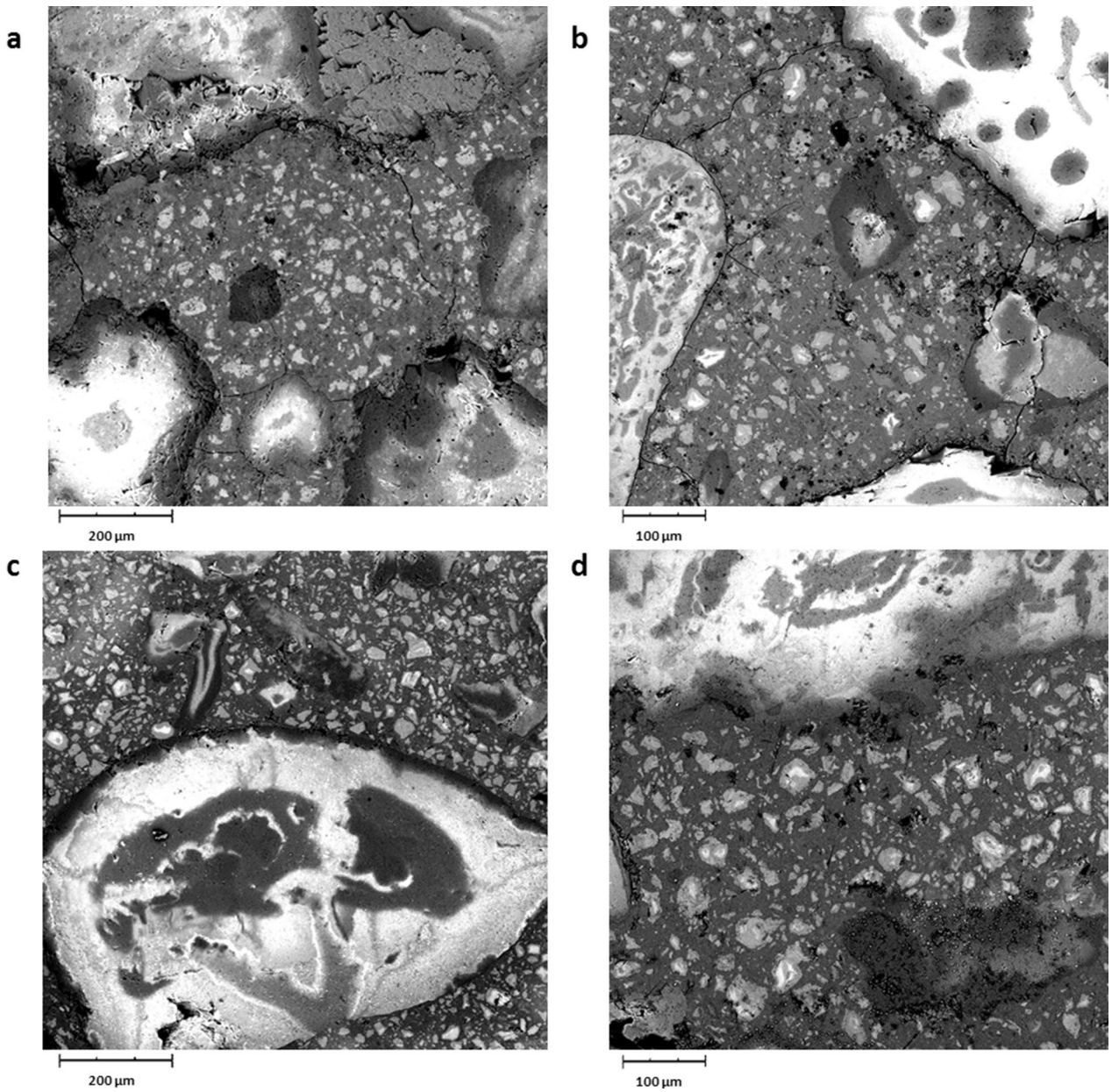

Fig. 11 SEM images: **a** with visible cracks radial to aggregates in irradiated samples, **b** with visible cracks along aggregate perimeter and radial cracks in irradiated samples, **c** and **d** without significant cracks in control samples.

(Reches 2019a). This means that aggregates and their constraining effect play the primary role in the microcrack formation in the cement mortar samples. This may explain the reason why the cement paste samples, for example, in Robira et al. (2018) and Maruyama et al. (2018) did not show any change in strength or showed only an insignificant change in strength.

Additionally to this finding, the results published by Khmurovska et al. (2019b) can be taken into consideration, which are the compressive strength reduction (observed through compressive strength test in Khmurovska et al. (2019b)) and a slight increase in creep (observed through direct measurements in Khmurovska et al. (2019b)) of irradiated samples.

All these observed changes may be caused by the water evaporation due to the gamma heating (Reches 2019b) and gas release due to the water radiolysis. Therefore, the prolonged exposure to gamma-ray

irradiation has an effect similar or equal to natural drying and/or heating (Maruyama et al. 2017) even in this case, when the carbonation reaction was not detected, and despite the rather small gamma heating (about 2 °C according to the short-term laboratory measurements) and the reportedly insignificant volume of released gases due to radiolysis (Ishikawa et al. 2019). The radiation-induced drying and/or heating then helps to explain the microcrack formation which leads to the observed porosity increase and the reduction of the compressive strength, which was intensified by the size effect (20% on average for the sample with the cross-section of 10×10 mm, (Khmurovska et al. 2019b)). The slight increase in creep of irradiated samples, which was observed by Khmurovska et al. (2019b), was also the consequence of drying and/or heating, which lead to microcrack formation and subsequently reduced the elastic modulus and resulted in higher creep (William et al. 2013), which was also intensified by the size effect.

The pore size distribution of not loaded samples is shown in Fig. 12a where it can be seen that the volume of pores of the irradiated samples (red) is increased with only the slight change in the peak position of pore size distribution in comparison with the control samples (blue). Nevertheless, the change in the peak position indicates the pore structure rearrangement. The cumulative curves of pore size distribution are shown in Fig. 13.

However, the irradiation brings the significant changes in the pore size distribution of the loaded samples, as can be seen in Fig. 12b. The maximum peak of the irradiated loaded samples (red) is shifted from 10–100 nm to a higher pore size (100–1000 nm, up to 10,000 nm for some samples) in comparison with the loaded control samples (blue). This means that the sustained load suppresses the development of the new pores and cracks while the already existing pores and cracks increase in size under irradiation.

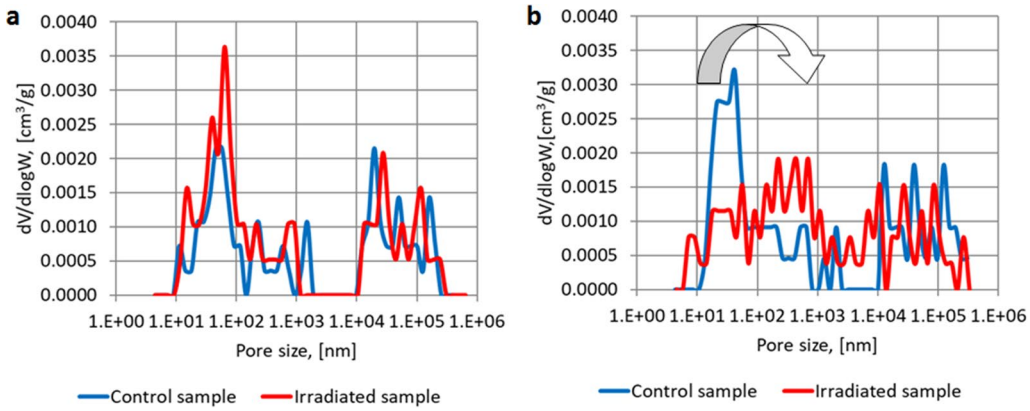

Fig. 12 Pore size distribution: **a** not loaded samples, **b** loaded samples.

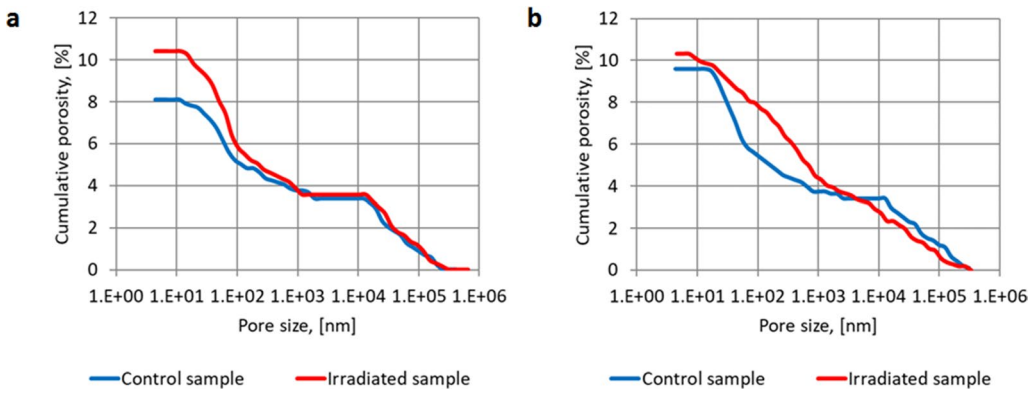

Fig. 13 Cumulative curves of pore size distribution: **a** not loaded samples, **b** loaded samples.

3.6 Effect of Superplasticizer

The influence of gamma-ray irradiation on superplasticizer and superplasticizer-containing cement paste is very complex and not fully understood yet, as the majority of the available researches do not provide any discussion regarding its possible effect (Reches, 2019a; Maruyama et al. 2017; Vodák et al. 2011). Generally, polycarboxylate consists of double bonded oxygen atoms so it is likely that some cross-linking takes place around these oxygen atoms. On the other hand, it is also possible that oxygen gas was generated during radiolysis of the polycarboxylate while main chain scissions occurred. Both of these effects potentially may change the properties of the superplasticizer and superplasticizer-containing cement paste.

However, the weight of the superplasticizer is about 0.3% of the total weight of the mortar in this study, therefore its potential effect on the properties of the gamma-ray irradiated mortar is considered to be negligibly small.

Nevertheless, an additional experiment with the analysis of the released gases and various amounts of superplasticizer may help to understand a possible effect of gamma-ray irradiation on a superplasticizer itself and superplasticizer-containing cement pastes.

4 Conclusions

Assuming that the results published by Khmurovska et al. (2019b) together with the research presented in this paper create a full set of experimental data obtained on the identical samples under the same experimental conditions, the knowledge about the effect of gamma-ray irradiation on cement mortar can be extended.

Besides the compressive strength reduction [observed through direct compressive strength test in (Khmurovska et al. 2019b)], and the slight increase in creep [observed through direct measurements in (Khmurovska et al. 2019b)] of irradiated samples, the newly added knowledge is:

(1) The indentation creep compliance and the indentation elastic modulus of C–S–H gel, which was investigated using nanoindentation technique, is affected negligibly by gamma-ray irradiation.

(2) No significant effect of gamma-ray irradiation on the cement mortar mineral composition is evidenced with XRD analysis results.

(3) The irradiation leads to the increase in porosity due to the pore structure rearrangement and microcrack occurrence.

(4) The sustained load suppresses the development of new pores and cracks while the already existing pores and cracks increase in size under irradiation.

(5) The radiation-induced increase of porosity may lead to a significant compressive strength reduction which was observed in previous study (Khmurovska et al. 2019b).

Now, with this new information and based on the data on the porosity of dried cement mortar available in literature, it is possible to conclude that the effect of gamma-ray radiation with the dose rate in the range from 3.90 to 4.71 kGy/h up to the dose of 15 MGy has a similar effect on the mechanical properties of hardened cement mortar as drying as it leads to the identical porosity increase in magnitude.

Supplementary Information

The online version contains supplementary material available at https://doi.org/10.1186/s40069-020-00452-7.

Additional file 1.
Additional file 2 .
Additional file 3.
Additional file 4.
Additional file 5.
Additional file 6.
Additional file 7.
Additional file 8.

Acknowledgements
The Joint Institute for Power and Nuclear Research—Sosny of the National Academy of Sciences of Belarus, Minsk, is gratefully acknowledged for performing the irradiation.

Author's informations
Yuliia Khmurovska is Researcher, Department of Concrete and Masonry Structures, Faculty of Civil Engineering Czech Technical University in Prague, Prague 166 29, Czech Republic. Petr Štemberk is a Professor, Department of Concrete and Masonry Structures, Faculty of Civil Engineering Czech Technical University in Prague, Prague 166 29, Czech Republic. Svyatoslav Sikorin is a Head of Laboratory of Experimental Physics and Nuclear Safety of Reactor Facilities, The Joint Institute for Power and Nuclear Research - Sosny of the National Academy of Sciences of Belarus, Minsk 220109, Belarus. Jiří Němeček is a Ph.D. student, Department of Mechanics, Faculty of Civil Engineering Czech Technical University in Prague, Prague 166 29, Czech Republic. Daria Jóźwiak-Niedźwiedzka is a Associate professor, Department of Experimental Mechanics, Institute of Fundamental Technological Research, Polish Academy of Sciences, Warsaw 02-106, Poland. Magdaléna Doleželová is a Researcher, Department of Materials Engineering and Chemistry, Faculty of Civil Engineering Czech Technical University in Prague, Prague 166 29, Czech Republic. Yuliya Kaladkevich is a Researcher, The Joint Institute for Power and Nuclear Research - Sosny of the National Academy of Sciences of Belarus, Minsk 220109, Belarus. Eryk Pavalanski is a Researcher, The Joint Institute for Power and Nuclear Research - Sosny of the National Academy of Sciences of Belarus, Minsk 220109, Belarus. Viktar Fatseyeu is a Researcher, The Joint Institute for Power and Nuclear Research - Sosny of the National Academy of Sciences of Belarus, Minsk 220109, Belarus.

Author's contributions
Yuliia Khmurovska under supervision of Petr Štemberk was responsible for the whole research including the design of the experiment and the analysis of the obtained data. Svyatoslav Sikorin together with Yuliya Kaladkevich, Eryk Pavalanski and Viktar Fatseyeu were responsible for the sample irradiation. Jiří Němeček was responsible for the nanoindentation tests and SEM

investigation, Daria Jóźwiak-Niedźwiedzka was responsible for the X-ray diffraction analysis, Magdaléna Doleželová was responsible for the mercury intrusion porosimetry (MIP).

Funding
This work was supported by Ministry of Education, Youth and Sports of Czech Republic, project 8F17002, the Technology Agency of the Czech Republic, project TJ04000186 and the Czech Technical University in Prague, project SGS20/043/OHK1/1T/11, which are gratefully acknowledged. The financial support of the National Centre for Research and Development of Poland, Project V4-Korea/2/2018 and of the European Commission, Euratom research and training programme 2014-2018 project No 900012—ACES—Towards Improved Assessment of Safety Performance for LTO of Nuclear Civil Engineering Structures, is also gratefully acknowledged.

Availability of Data and materials
Please contact author for data requests.

Competing interests
The authors declare that they have no competing interests.

Author details
[1] Department of Concrete and Masonry Structures, Faculty of Civil Engineering, Czech Technical University in Prague, Prague 166 29, Czech Republic. [2] Laboratory of Experimental Physics and Nuclear Safety of Reactor Facilities, The Joint Institute for Power and Nuclear Research, Sosny of the National Academy of Sciences of Belarus, 220109 Minsk, Belarus. [3] Department of Mechanics, Faculty of Civil Engineering, Czech Technical University in Prague, Prague 166 29, Czech Republic. [4] Department of Experimental Mechanics, Institute of Fundamental Technological Research, Polish Academy of Sciences, 02-106 Warsaw, Poland. [5] Department of Materials Engineering and Chemistry, Faculty of Civil Engineering, Czech Technical University in Prague, Prague 166 29, Czech Republic. [6] The Joint Institute for Power and Nuclear Research, Sosny of the National Academy of Sciences of Belarus, 220109 Minsk, Belarus.

Received: 9 July 2020 Accepted: 2 December 2020
Published online: 03 March 2021

References

ACI Code Committee. (2008). Guide for modeling and calculating shrinkage and creep in hardened concrete. ACI Committee 209 (ACI 209.2R-08), American Concrete Institute, Farmington Hills, MI. http://www.civil.northwestern.edu/people/bazant/PDFs/Papers/R21.pdf.

Bažant, Z. P., & Jirásek, M. (2018). *Creep and hygrothermal effects in concrete structures* (Vol. 38). Dordrecht, The Netherlands: Springer.

CEB-FIP. (1991). Model code 1990: Final Draft - Vol. 3. CEB-Bulletind'Information 203-205. Comite Euro-International Du Beton, Lausanne, Swizerland. https://books.google.cz/books/about/CEB_FIP_Model_Code_1990.html?id=N-VDAQAAIAAJ&redir_esc=y.

Chen, Y., Liu, P., & Yu, Z. (2018). Effects of environmental factors on concrete carbonation depth and compressive strength. *Materials, 11*(11), 2167.

Denisov, A., Dubrovskii, V., & Solovyov, V. (2012). *Radiation resistance of mineral and polymer construction materials*. Moscow: ZAO MEI Publ. House. **(In Russian)**.

Dubrovskii, V., Lavdanskii, P., & Engovatov, I. (2010). *Construction of nuclear power plants*. Moscow: Publishing Association of Civil Engineering Universities. **(In Russian)**.

Elsalamawy, M., Mohamed, A. R., & Kamal, E. M. (2019). The role of relative humidity and cement type on carbonation resistance of Concrete. *Alexandria Engineering Journal, 58*(4), 1257–1264.

Gardner, N. J., & Lockman, M. J. (2001). Design provisions for drying shrinkage and creep of normal-strength concrete. *Materials Journal, 98*(2), 159–167.

Gray, B. S. (1972). *The effect of reactor radiation on cements and concrete* (pp. 17–39). Luxembourg: Comm. of the European Communities.

Hilloulin, B., Robira, M., & Loukili, A. (2018). Coupling statistical indentation and microscopy to evaluate micromechanical properties of materials: Application to viscoelastic behavior of irradiated mortars. *Cement and Concrete Composites, 94,* 153–165.

Hilsdorf, H. K., Kropp, J., & Koch, H. J. (1978). The effects of nuclear radiation on the mechanical properties of concrete. *Special Publication, 55,* 223–254.

Ishikawa, S., Maruyama, I., Takizawa, M., Etoh, J., Kontani, O., & Sawada, S. (2019). Hydrogen production and the stability of hardened cement paste under gamma irradiation. *Journal of Advanced Concrete Technology, 17*(12), 673–685.

Khmurovska, Y., Štemberk, P., Fekete, T., & Eurajoki, T. (2019a). Numerical analysis of VVER-440/213 concrete biological shield under normal operation. *Nuclear Engineering and Design, 350,* 58–66.

Khmurovska, Y., Štemberk, P., Sikorin, S., Žák, J., Khaladkevich, Y., Pavalanski, E., & Fatseyeu, V. (2019b). Cement mortar creep under exposure to gamma-ray irradiation. *Journal of Nuclear Research and Development, 18,* 24–28.

Lowinska-Kluge, A., & Piszora, P. (2008). Effect of gamma irradiation on cement composites observed with XRD and SEM methods in the range of radiation dose 0–1409 MGy. *Acta Physica Polonica-Series A General Physics, 114*(2), 399.

Maruyama, I., Kontani, O., Takizawa, M., Sawada, S., Ishikawao, S., Yasukouchi, J., & Igari, T. (2017). Development of soundness assessment procedure for concrete members affected by neutron and gamma-ray irradiation. *Journal of Advanced Concrete Technology, 15*(9), 440–523.

Maruyama, I., Ishikawa, S., Yasukouchi, J., Sawada, S., Kurihara, R., Takizawa, M., & Kontani, O. (2018). Impact of gamma-ray irradiation on hardened white Portland cement pastes exposed to atmosphere. *Cement and Concrete Research, 108,* 59–71.

McDowall, D. C. (1971). The effect of gamma irradiation on the creep properties of concrete. In: Proceedings of an information exchange meetingon results of concrete irradiation programmes, volume EUR 4751 f-e.Brussels, Belgium, 19 April, 1971. Brussels: Commission des CommunautéesEuropéennes.

Minster, J., Blahova, O., Lukes, J., & Nemecek, J. (2010). Time-dependent mechanical characteristics measured through the use of a microindentation technique. *Mechanics of Time-Dependent Materials, 14*(3), 243–251.

Nokken, M. R., & Hooton, R. D. (2008). Using pore parameters to estimate permeability or conductivity of concrete. *Materials and Structures, 41*(1), 1.

Oliver, W. C., & Pharr, G. M. (1992). An improved technique for determining hardness and elastic modulus using load and displacement sensing indentation experiments. *Journal of Materials Research, 7*(6), 1564–1583.

Oliver, W. C., & Pharr, G. M. (2004). Measurement of hardness and elastic modulus by instrumented indentation: Advances in understanding and refinements to methodology. *Journal of Materials Research, 19*(1), 3–20.

Reches, Y. (2019a). A multi-scale review of the effects of gamma radiation on concrete. *Results in Materials, 2,* 100039.

Reches, Y. (2019b). Quantification and modeling of the interactions of gamma radiation with concrete from bulk-scale observations. *International Journal of Concrete Structures and Materials, 13*(1), 59.

Robira, M., Hilloulin, B., Loukili, A., Potin, G., Bourbon, X., & Abdelouas, A. (2018). Multi-scale investigation of the effect of γ irradiations on the mechanical properties of cementitious materials. *Construction and Building Materials, 186,* 484–494.

Shimizu, S., Yanagimoto, T., & Sakai, M. (1999). Pyramidal indentation load–depth curve of viscoelastic materials. *Journal of Materials Research, 14*(10), 4075–4086.

Soo, P., & Milian, L. M. (2001). The effect of gamma radiation on the strength of Portland cement mortars. *Journal of Materials Science Letters, 20*(14), 1345–1348.

Taerwe, L., & Matthys, S. (2013). *Fib model code for concrete structures 2010*. Berlin: Ernst & Sohn Wiley.

Tajuelo, E. R., Hunnicutt, W. A., Mondal, P., & Le Pape, Y. (2018). Assessing the effects of gamma irradiation in concrete. *Transactions, 118*(1), 1649–1650.

Tajuelo, E. R., Hunnicutt, W. A., Mondal, P., & Le Pape, Y. (2020). Examination of gamma-irradiated calcium silicate hydrates Part I: Chemical-structural properties. *Journal of the American Ceramic Society, 103*(1), 558–568.

Vaitová, M., Štemberk, P., Petřík, M., Žďárek, J., & Chvála, O. (2018). Structural aspect of corium spill on VVER-1000 reactor pit floor slab. *Progress in Nuclear Energy, 107,* 148–154.

Vodák, F., Trtík, K., Sopko, V., Kapičková, O., & Demo, P. (2005). Effect of γ-irradiation on strength of concrete for nuclear-safety structures. *Cement and Concrete Research, 35*(7), 1447–1451.

Vodák, F., Vydra, V., Trtík, K., & Kapičková, O. (2011). Effect of gamma irradiation on properties of hardened cement paste. *Materials and Structures, 44*(1), 101–107.

William, K., Xi, Y., & Naus, D. (2013). *A review of the effects of radiation on microstructure and properties of concretes used in Nuclear Power Plants*. Tech. Rep. NUREG/CR-7171 ORNL/TM2013/263, United StatesNuclear Regulatory Commission, Oak Ridge National Laboratory.

Publisher's Note